

1 DeepMIP-Eocene-p1: multi-model dataset and 2 interactive web application for Eocene climate 3 research

4 Sebastian Steinig^{1,*}, Ayako Abe-Ouchi², Agatha M. de Boer³, Wing-Le Chan², Yannick
5 Donnadieu⁴, David K. Hutchinson^{3,5}, Gregor Knorr⁶, Jean-Baptiste Ladant⁷, Polina
6 Morozova⁸, Igor Niezgodzki^{6,9}, Christopher J. Poulsen¹⁰, Evgeny M. Volodin¹¹, Zhongshi
7 Zhang^{12,13}, Jiang Zhu¹⁴, David Evans¹⁵, Gordon N. Inglis¹⁵, A. Nele Meckler¹⁶, and Daniel J.
8 Lunt¹

9 ¹School of Geographical Sciences, University of Bristol, UK

10 ²Atmosphere and Ocean Research Institute, University of Tokyo, Kashiwa, Japan

11 ³Department of Geological Sciences, Stockholm University, Sweden

12 ⁴Aix Marseille Univ, CNRS, IRD, INRA, Coll France, CEREGE, Aix-en-Provence, France

13 ⁵Climate Change Research Centre, University of New South Wales Sydney, Sydney, Australia

14 ⁶Alfred Wegener Institute, Helmholtz Centre for Polar and Marine Research, Bremerhaven, Germany

15 ⁷Laboratoire des Sciences du Climat et de l'Environnement, LSCE/IPSL, CEA-CNRS-UVSQ, Université
16 Paris-Saclay, Gif-sur-Yvette, France

17 ⁸Institute of Geography, Russian Academy of Sciences, Moscow, Russia

18 ⁹ING PAN - Institute of Geological Sciences Polish Academy of Sciences, Research Center in Kraków,
19 Biogeosystem Modelling Group, Kraków, Poland

20 ¹⁰Department of Earth Sciences, University of Oregon, Eugene, Oregon, USA

21 ¹¹Institute of Numerical Mathematics, Russian Academy of Sciences, Moscow, Russia

22 ¹²NORCE Norwegian Research Centre, Bjerknes Centre for Climate Research, Norway

23 ¹³Department of Atmospheric Science, School of Environmental Studies, China University of Geosciences, Wuhan,
24 China

25 ¹⁴Climate & Global Dynamics Laboratory, National Center for Atmospheric Research, USA

26 ¹⁵School of Ocean and Earth Science, University of Southampton, UK

27 ¹⁶Bjerknes Centre for Climate Research and Department of Earth Science, University of Bergen, Norway

28 *corresponding author: Sebastian Steinig (sebastian.steinig@bristol.ac.uk)

29 ABSTRACT

Paleoclimate model simulations provide reference data to help interpret the geological record and offer a unique opportunity to evaluate the performance of current models under diverse boundary conditions. Here, we present a dataset of 35 climate model simulations of the warm early Eocene Climatic Optimum (EECO; ~ 50 million years ago) and corresponding preindustrial reference experiments. To streamline the use of the data, we apply standardised naming conventions and quality checks across eight modelling groups that have carried out coordinated simulations as part of the Deep-Time Model Intercomparison Project (DeepMIP). Gridded model fields can be downloaded from an online repository or accessed through a new web application that provides interactive data exploration. Local model data can be extracted in CSV format or visualised online for streamlined model-data comparisons. Additionally, processing and visualisation code templates may serve as a starting point for advanced analysis. The dataset and online platform aim to simplify accessing and handling complex data, prevent common processing issues, and facilitate the sharing of climate model data across disciplines.

31 Background & Summary

32 Past climate changes provide an opportunity to better understand how key components of the climate system might change under
33 anthropogenic greenhouse gas emissions and thus help constrain future climate change¹. Comparisons with paleoclimate data

34 allow us to evaluate climate models under atmospheric CO₂ scenarios similar to those possible in the near future. Furthermore,
35 these paleoclimate model simulations provide global, physically consistent reference data to support the interpretation of
36 paleoclimatic data across a wide range of disciplines, e.g. in geology, biology, and geochemistry.

37
38 One of the most well-studied deep-time intervals with respect to model-data comparison is the early Eocene Climatic
39 Optimum (EECO; ~53.3 to 49.1 million years ago²) as it provides an analogue for future very high emission scenarios³. It was
40 characterised by atmospheric CO₂ concentrations of ~1,500 ppmv⁴ and global mean surface temperatures (GMSTs) 10 to 16
41 °C warmer than pre-industrial⁵. Several modelling studies have focused on improving our understanding of the mechanisms and
42 implications of EECO warmth^{6–10} and ultimately motivated the formulation of the Eocene Modelling Intercomparison Project
43 (EoMIP)¹¹. While limited due to its opportunistic design, EoMIP nonetheless highlighted the possibility of using multi-model
44 ensembles to systematically assess model-model and model-data differences in our understanding of Eocene climate.

45
46 Building on this potential, DeepMIP – the Deep-Time Model Intercomparison Project – was designed to provide a consistent
47 framework to carry out coordinated EECO model experiments¹². Eight modelling groups performed a total of 35 model
48 simulations using the same paleogeographic and vegetation boundary conditions at a range of atmospheric CO₂ concentrations
49 (Table 1). These new simulations showed more consistent global mean surface temperatures across the ensemble and larger
50 climate sensitivities compared to the EoMIP results¹³. The coordinated experiment set-up allowed a separation of the relative
51 influence of changes in CO₂ concentrations and non-CO₂ boundary conditions (i.e. removal of land ice and prescribed
52 vegetation) on the simulated surface temperatures. Non-CO₂ boundary conditions alone lead to 3-5 °C overall warming and
53 contribute substantially to the reduced meridional temperature gradient, while higher CO₂ levels drive global mean warming
54 due to decreases in atmospheric emissivity. Importantly, three models (CESM1.2-CAM5, GFDL-CM2.1 and NorESM1-F)
55 were able to produce absolute GMSTs and reduced meridional temperature gradients consistent with the geological record at
56 CO₂ concentrations within the reported range of EECO reconstructions (1170 to 2490 ppmv¹⁴).

57
58 The DeepMIP-Eocene ensemble has already been used in multiple studies, analysing specific aspects of the Eocene
59 climate in more detail, e.g. the meridional temperature gradient¹⁵, the surface to deep ocean temperature relationship¹⁶,
60 ocean circulation¹⁷, sea ice¹⁸, hydroclimate^{19–21}, and the impact of mountains^{22,23}. We anticipate continued interest in the
61 DeepMIP-Eocene model data, both for model intercomparisons and for model-data syntheses, and aim to document the

62 design of the dataset and streamline access to improve future reuse of the data. Although the use of large model ensembles
63 is helpful in quantifying the influence of uncertainties in boundary conditions and limitations in model performance on the
64 simulated Eocene climate, it also presents a technical hurdle in accessing and fully utilising the available data. The use of
65 model-specific data standards, post-processing workflows and variable naming schemes can make the analysis and comparison
66 of multi-model ensembles a tedious process or even lead to processing errors. The need for significant data processing expertise
67 can therefore limit the benefits and wider use of these important data, particularly in non-modelling paleoclimatology disciplines.

68
69 Here, we build on the DeepMIP framework to address these issues and present standardised, quality-checked EECO model
70 output to facilitate multi-model processing and analysis, both for model intercomparisons and model-data comparisons. We
71 have reprocessed the output of a total of 26 EECO simulations at CO₂ concentrations between ×1 and ×9 pre-industrial levels,
72 together with their nine pre-industrial reference experiments, to generate a dataset of common climate variables with consistent
73 temporal averaging, variable names and units across the ensemble. We follow the CMIP convention for variable names and
74 units as closely as possible to take advantage of existing processing workflows, and use the ensemble spread to quantify the
75 internal consistency of the output fields.

76
77 We provide two complementary ways of accessing the dataset, tailored to the most likely future use cases. First, the entire
78 dataset is stored as global, gridded netCDF (network Common Data Form) files in the Centre for Environmental Data Analysis
79 (CEDA) Archive and can be downloaded as individual files or in batch mode²⁴. Combined with the consistent DeepMIP naming
80 convention, this provides a more traditional, scriptable starting point for further analysis. This approach shares the goals of
81 other existing infrastructure projects for sharing climate model data such as the Earth System Grid Federation (ESGF)²⁵, but the
82 limited scope and overall much smaller file sizes of this dataset allow us to use centralised, rather than distributed, data storage
83 for greater user convenience. Second, we present an interactive web application to facilitate model-data comparisons of EECO
84 surface temperatures and precipitation. This is a very common use case for paleoclimate model data, but also involves multiple
85 processing steps and potential pitfalls, especially when working with a large model ensemble. Modern web technologies
86 provide the opportunity for intuitive, browser-based access to complex data and, therefore, the possibility to assist users in
87 extracting subsets of relevant information for them. Recent examples include the Interactive Atlas²⁶ of the Intergovernmental
88 Panel on Climate Change (<https://interactive-atlas.ipcc.ch>, last access: 26 June 2024) and the Copernicus Interactive Climate
89 Atlas created by the Copernicus Climate Change Service (<https://atlas.climate.copernicus.eu/atlas>, last access: 26 June 2024).

90 The DeepMIP web application follows a similar approach by providing intuitive data access and custom workflows to simplify
91 common model-data comparison tasks. The web application automatically calculates paleolocations for a single site or a list of
92 present-day locations, extracts the corresponding model data from the various model grids and plots a summary of the results.
93 The resulting data can be exported for further offline analysis, while the underlying Python code can be used as a starting point
94 for custom analysis.

95
96 The dataset and tools provided are designed to enable data access for non-programmers and to streamline analysis for
97 more advanced users to routinely evaluate existing and emerging paleoclimate data against the full DeepMIP-Eocene model
98 ensemble. This will help to bridge the gap between modelling and data communities to ultimately advance our understanding of
99 early Eocene climate and could potentially serve as a reference framework for similar projects of other geological time periods
100 in the future.

101 **Methods**

102 **DeepMIP-Eocene experiments**

103 All EECO simulations that follow the DeepMIP-Eocene experimental design protocol¹² and are completed by September
104 2023 form the input data for version 1.0 of the dataset (Table 1). These simulations are identical to those described in the
105 DeepMIP overview paper¹³, with the exception of the new MIROC $\times 1$ and $\times 2$ experiments. The DeepMIP framework
106 provides standardised model boundary conditions and experimental designs to allow a coordinated model intercomparison
107 of the simulation results. All groups have used one of the two reference paleogeographic reconstructions^{27,28} (Fig. 1a-b)
108 interpolated to their respective model grids. The main difference between the two available paleogeographies is the choice in the
109 applied rotation reference frame leading to slight differences in the relative positions of individual plates (Fig. 1c). Prescribed
110 vegetation and river runoff follow a published reconstruction²⁷, while globally homogeneous soil parameters based on the
111 global mean of the respective pre-industrial simulation were used. All groups provided a pre-industrial reference simulation
112 and performed a series of EECO experiments, differing only in the concentration of atmospheric CO₂, summarised in Table 2.
113 Other greenhouse gas concentrations and the solar constant were held constant at their pre-industrial levels.

114
115 A complete overview of the modelling framework is given in the DeepMIP experimental design paper¹², and detailed
116 descriptions of its implementation in the individual models can be found in the analysis of the large-scale climatic features¹³.

117 We also provide a full description of each model setup based on their published method sections¹³ as a README file in the
118 dataset itself. This is intended to make the downloaded files self-describing and to allow dynamic addition of new experiments
119 and models in the future. In the following, for each model included in version 1.0 of the dataset, we provide a brief summary
120 of the initialisation and spin-up strategies, as this step required individual decisions by each modelling group. The DeepMIP
121 experimental design provides an idealised equation for initialising the ocean temperatures as:

$$T[^\circ\text{C}] = \begin{cases} \left(\frac{D-z}{D} \times A \times \cos(f)\right) + B & \text{if } z \leq D \text{ m} \\ B & \text{if } z > D \text{ m} \end{cases} \quad (1)$$

122 where f is latitude, and z is ocean depth. The parameters A , B and D are specified in the experimental design as 25, 15 and
123 5000, respectively¹². The resulting warm ocean temperatures caused numerical problems in some model spin-ups and have
124 therefore been modified for individual models. An overview of the parameters used for each model is given in Table 3. Any
125 other deviations for the model initialisation are listed below.

126 **CESM**

127 Ocean temperatures and salinities in all Eocene simulations are initialised from the same Palaeocene–Eocene Thermal Maximum
128 (PETM; ~55 million years ago) experiment using a previous version of CESM^{29,30}. The $\times 1$ simulation was integrated for a
129 further 2600 years, while all other experiments were run for 2000 years. The mean top of the atmosphere (TOA) imbalance over
130 the last 100 model years for the PI, $\times 1$, $\times 3$, $\times 6$ and $\times 9$ experiments are -0.05, -0.25, -0.32, 0.34 and 0.64 Wm^{-2} , respectively.

131 **COSMOS**

132 The $\times 3$ integration was initialised with a homogeneous temperature and salinity of 10 $^\circ\text{C}$ and 34.7 psu, respectively, and
133 integrated for an initial 1000 years, after which the $\times 1$ and $\times 4$ simulations were branched. After an initial 8000 years with
134 transient orbital parameters, a constant, pre-industrial orbital configuration was used for the final 1500 years of all simulations.
135 Instead of using the proposed river routing scheme²⁷, the simulations use a hydrological discharge model that follows the model
136 orography³¹. The mean TOA imbalance over the last 100 model years for the PI, $\times 1$, $\times 3$ and $\times 4$ experiments are 1.75, 1.91,
137 1.78, and 1.95 Wm^{-2} , respectively.

138 *GFDL*

139 The $\times 1$, $\times 2$, $\times 3$, and $\times 4$ simulations were started with a globally homogeneous salinity of 34.7 psu and a slightly cooler
140 version of the DeepMIP temperature equation (Eq. (1); Table 3). After 1500 and 2000 years of integration, an acceleration
141 technique was applied. Specifically, the linear temperature trends of the last 100 years for each model level below 500 m
142 calculated and the temperature then extrapolated by a 1000 years following this trend. After the second application of this
143 technique at year 2000, the model was run out normally for a further 4000 years for a total of 6000 years. The $\times 6$ simulation
144 was initialised with a globally uniform temperature of 19.32 °C and continuously integrated for 6000 years. The mean TOA
145 imbalance over the last 100 model years for the PI, $\times 1$, $\times 2$, $\times 3$, $\times 4$ and $\times 6$ experiments are 0.31, 0.10, -0.08, -0.14, -0.19, and
146 -0.28 Wm^{-2} , respectively.

147 *HadCM3*

148 Initial ocean temperatures for HadCM3BL were derived from an idealised temperature profile with lowered, CO₂ dependent
149 deep ocean temperatures based on previous Eocene simulations. HadCM3B experiments were branched from the respective
150 HadCM3BL simulations after 4400 to 4900 years and integrated for a further 2950 years. Multiple ocean gateways in the
151 original paleogeography were widened to allow unrestricted ocean circulation and to guarantee the same gateway widths on
152 both the low and high-resolution ocean grids of HadCM3BL and HadCM3B, respectively. In addition, maximum water depths
153 in parts of the Arctic Ocean were reduced to improve numerical stability. The mean TOA imbalance per century averaged
154 over the last 50 model years for the PI, $\times 1$, $\times 2$ and $\times 3$ experiments for HadCM3B are -0.04, -0.02, -0.08 and -0.08 Wm^{-2} ,
155 respectively.

156 *INMCM*

157 The ocean temperature and salinity in the $\times 6$ simulation follow the idealised equations of the DeepMIP protocol, but with
158 equatorial surface temperatures lowered by 5 °C (Eq. (1); Table 3). The simulation was integrated for a total of 1150 years. The
159 mean TOA imbalance over the last 100 model years for the PI and $\times 6$ experiments are 4.37 and 2.87 Wm^{-2} , respectively.

160 *IPSL*

161 A modified version of Eq. (1) with overall reduced subsurface temperatures (Table 3) and a globally homogeneous salinity of
162 34.7 psu were used to initialise the $\times 3$ simulation. The $\times 1.5$ simulation is branched from the $\times 3$ experiment after 1500 years.
163 Both simulations are run for a total of 4000 years. The ocean bathymetry around individual ocean straits has been manually
164 adjusted to guarantee the minimum gateway width necessary to allow throughflow. The mean TOA imbalance over the last 100

165 model years for the PI, $\times 1.5$ and $\times 3$ experiments are 0.08, 0.59 and 0.76 Wm^{-2} , respectively.

166 **MIROC**

167 All three simulations have been initialised with a modified version of the idealised DeepMIP temperature equation, with ocean
168 temperatures globally reduced by $15 \text{ }^\circ\text{C}$ (Eq. (1); Table 3), and integrated for 5000 model years. The $\times 1$ and $\times 2$ experiments
169 are new and have not been included in the DeepMIP overview paper¹³. The mean TOA imbalance over the last 100 model
170 years for the PI, $\times 1$, $\times 2$ and $\times 3$ experiments are 0.96, 0.79, 0.91 and 0.96 Wm^{-2} , respectively.

171 **NorESM**

172 Initial ocean temperatures for the $\times 2$ simulation were used from a previous NorESM-L simulation³², while salinities were set to
173 25.5 psu in the Arctic and 34.5 elsewhere. The $\times 4$ simulation was branched off after 100 model years, and both simulations have
174 been run for a further 2000 years. The NorESM simulations were performed with a different paleogeographic reconstruction
175 than the rest of the DeepMIP ensemble (Table 1). The mean TOA imbalance per century at the end of the PI, $\times 2$ and $\times 4$
176 experiments are -0.02 , 0.03 and 0.24 Wm^{-2} , respectively. Note that the PI imbalance is calculated over the last 1000 years,
177 while the Eocene values are averaged over the last 100 years.

178 **Data processing**

179 We use the raw output of the last 100 years of each of the 35 model simulations as input for our post-processing. For each
180 variable, we generate up to three netCDF output files to facilitate common analysis workflows. We always produce a mean file
181 representing either the monthly mean climatology or the annual mean averaged over the last 100 model years, depending on the
182 temporal resolution of the model output. In case of monthly mean output data, the `std` file contains the standard deviation over
183 the same averaging period for each month of the year and can be used for significance testing. Where feasible, we also store the
184 full monthly mean output of the last 100 model years as a `time_series` file to investigate temporal trends or interannual
185 variability.

186
187 Alongside this standard output, we provide a generic script to interpolate model fields from their native grids to a common
188 resolution for model intercomparisons. The processing workflow requires a local installation of the Climate Data Operator
189 (CDO) software³³ for bilinear or nearest-neighbour interpolation for atmosphere and ocean variables, respectively. Example
190 output for commonly used variables (i.e., near-surface air temperature, sea surface temperature and total precipitation) on a
191 common $1^\circ \times 1^\circ$ grid is included in the dataset and can be directly used for analysis or to verify results of any local postprocessing.

192 The processing script is distributed as part the dataset (see Data Records section).

193 Naming convention

194 We employ a consistent naming convention for variables, directories, and file names across all models to simplify the comparison
195 of different models and to allow a scripted analysis of the entire dataset. The list of output variables is an extended version
196 of those proposed in the DeepMIP experimental design¹² and is shown in Tables 4-5. Variable names, units and signs of
197 fluxes follow the naming convention of the Coupled Model Intercomparison Project 6 (CMIP6) data request (https://wcrp-cmip.github.io/WGCM_Infrastructure_Panel/CMIP6/data_request.html, last access: 26 June 2024). Consistent standard names,
198 long names and global attributes are directly added to the netCDF files following the Climate and Forecast metadata conventions
199 (CF³⁴) in version 1.8 (<http://cfconventions.org>, last access: 26 June 2024). All netCDF files have been automatically tested for
200 CF-compliance with the cf-checker utility (<https://github.com/cedadev/cf-checker>, last access: 26 June 2024) developed by
201 the UK Met Office and the NCAS Computational Modelling Services (NCAS-CMS). Following the CMIP and CF community
202 standards will both increase user familiarity with the new dataset and will allow the integration into existing analysis workflows
203 and software. Each output variable is stored in a separate file according to the following structure:

205 directory = deepmip-eocene-p1/<Family>/<Model>/<Experiment>/<Version>/<Averaging>/

206

207 filename = <Variable>_<Model>_<Experiment>_<Version>.<Statistic>.nc

208 where:

- 209 • <Family> , <Model> and <Experiment> are listed in Table 1 and Table 2, respectively
- 210 • <Variable> represents the first column in Tables 4-5
- 211 • <Statistic> is either mean (1 or 12 timesteps) std (12 timesteps) time_series (1200 timesteps) or omitted for
212 the time-independent boundary conditions
- 213 • the smaller mean and std files are stored in the <Averaging>=climatology directory and are separated from
214 the larger time_series files in the <Averaging>=time_series directory to enable more granular download
215 options

216 Storing all relevant information in the file name itself also allows new phases of coordinated DeepMIP simulations to be
217 integrated into a single dataset in the future.

218 Data Records

219 The full dataset has been deposited in the CEDA Archive, the UK national data centre for atmospheric and earth observation
220 research²⁴. This dataset contains the following types of files:

- 221 • model data: The directory `deepmip-eocene-p1` contains all processed model output in CF compliant netCDF
222 format³⁵, a self-describing community standard for storing gridded simulation data, with a total file size of 168.0 GB.
223 Directory and file structure follow the DeepMIP naming convention described above.
- 224 • model READMEs: Each `<Family>` top-level directory contains a single `<Family>_README.md` file that contains
225 detailed information about the model, the simulation setup, and naming convention. This ensures the downloaded dataset
226 is sufficiently self-described and allows the addition of new models and simulation results in the future.

227 In addition, the code of the web application³⁶ and a collection of scripts and metadata to interact with the dataset³⁷ are
228 deposited in separate Zenodo repositories. The latter includes a collection of Python code to interpolate model data to a
229 common grid (`egrid_deepmip_data.py`), recreate the validation tables of available data (`plot_z-scores.py`) and
230 Python dictionaries containing available DeepMIP models, experiments and variables to support scripted analysis of the dataset
231 (`deepmip-eocene_dictionaries_v1.py`).

232 Technical Validation

An earlier version of the dataset has already been used in a number of publications^{13-15, 16, 18-23} to assess the scientific validity of the model simulations, both in terms of model-model and model-data comparisons. In this section, we verify the internal consistency of the dataset, ensuring that the naming convention has been applied correctly and that the resulting variable names, units and fluxes are consistent across all models. To do this, we automatically parse all `time_series` files in the dataset for any given experiment, interpolate them to a common grid, calculate the global mean, minimum and maximum values and compare these values across all models. We use annual mean fields for the validation of data and the last 12 available months of the `time_series` files. For variables with multiple vertical levels (see Tables 4-5), we select the vertical index nearest to the 500 hPa pressure level or 1000 m depth for atmospheric and ocean data, respectively. Example tables for atmospheric and ocean mean variables from the 3 simulations are shown in Fig. 2 and Fig. 3, tables for all other experiments as well as for `time_series` files are uploaded to the online dataset and web application. This testing procedure simulates a standard analysis workflow and is able to detect any deviations from the expected DeepMIP naming convention, while the

resulting tables provide a visual overview of the available model fields for each experiment. We further calculate the median and standard deviation for each variable and metric across all available models (i.e. for each row in the table) to flag potential outliers that may arise due to inconsistent units or different directions of energy or mass fluxes. For this, we calculate a z-score for each model, variable and statistic which quantifies the number of standard deviations an individual model statistic is above or below the ensemble median. We use the ensemble median instead of the mean as the reference point to reduce the influence of potential outliers in our small sample sizes and calculate the adjusted z-scores as:

$$z = \frac{x - M}{s} \quad (2)$$

where z is the computed z-score, x is the individual model value, M is the median across all available models for the respective variable and statistic (i.e., across each table row), and s is the standard deviation across the ensemble. A z-score > 3 is commonly used as a cut-off to identify outliers in a distribution. Due to the small sample sizes (the z-score threshold was not used to exclude any data from the dataset, but rather to find and resolve inconsistencies in the data processing between the models. For this, the background of each cell in Fig. 2 and Fig. 3 has been coloured by their computed z-score to visually identify model results substantially different from the ensemble median. Note that all modelling groups have performed slightly different sets of simulations (Table 1) and not all models provide all requested output variables. These fields are indicated by gray "nan" cells in the overview tables. For example, INM and NorESM did not perform an experiment and are therefore not included in Fig. 2 and Fig. 3. In the final dataset, all available model fields are within 3 standard deviations around the respective ensemble median, although we note that the small sample sizes allow only an indicative analysis. The Python processing code is included in the online dataset (see Data Records section) and can be used to develop a custom analysis workflow or to validate any regridding and global averaging performed by the user.

Usage Notes

We present two primary routes to access the dataset, either via downloading the netCDF files for local processing or via an interactive website for online model-data comparisons.

netCDF repository

First, processed netCDF files for all simulations are available from the CEDA Archive. The full directory structure can be accessed via the browser and files can be downloaded via HTTP, Wget, FTP or OPeNDAP. This allows easy access to the data

251 via the browser, as well as scriptable interfaces for bulk downloading. The OPeNDAP (Open-source Project for a Network Data
252 Access Protocol) protocol allows the remote subsetting and exploration of datasets directly in Python, R, IDL, and Matlab.
253 The CEDA Archive website (<https://help.ceda.ac.uk/article/99-download-data-from-ceda-archives>; last access: 26 June 2024)
254 provides an up-to-date overview of all available access options.

255 256 Interactive web application

257 Second, simulated surface temperatures and precipitation from any location can be extracted, visualised and downloaded at
258 <https://data.deepmip.org>. This allows model-data comparisons via a simple user interface without the need to download the
259 netCDF files locally. The website is designed to extract surface temperature and precipitation for any user-defined location
260 from all available model simulations and either visualise the results or download them for offline use. All processing code is
261 written in Python and bundled into a web application via the Streamlit library (<https://streamlit.io>; last access: 26 June 2024).
262 The code makes full use of the naming conventions described above and is therefore general enough to serve as a template for
263 further in-depth analysis. The sidebar of the web application can be used to choose between three different analysis pages:

264 1. Extract local model data: Finds the model data closest to a user-specified site (see example in Fig. 4). The minimum
265 inputs are the modern location of the site and the variable of interest (either near-surface air temperature, sea surface
266 temperature, or total precipitation). The application will automatically reconstruct the site's EECO paleo-position on both
267 the mantle²⁷ and paleomagnetic²⁸ reference frames and extract the respective monthly and annual mean simulation data
268 from the closest grid point for all models in the dataset. Model data is interpolated to a common grid (see Data
269 processing section for details) prior to the data selection to eliminate the influence of different model resolutions on the
270 results. In the end, the ensemble means for each experiment are calculated and the results are listed in an interactive table.
271 Data can be downloaded in CSV, Excel or JSON format for direct import into spreadsheets for further offline analysis.
272 The extraction can be performed for a single site or a list of locations and all sites from the DeepMIP proxy³ dataset
273 are pre-loaded and available for comparison with the simulation results. Furthermore, the underlying Python functions
274 `get_paleo_locations()` and `get_model_point_data()` are available in the `deepmip_modules.py` file
275 of the application repository for reuse in any custom analysis. The `get_paleo_locations()` function uses the
276 paleolocation lookup fields provided in the experimental design paper¹³ and the respective early Eocene locations
277 for a list of modern latitude/longitude pairs, using both the mantle²⁷ and paleomagnetic²⁸ reference frames. Results are

278 saved in a Pandas DataFrame which can be directly passed to `model_point_data()` to extract the nearest
279 model data for all reconstructed locations.

280 2. Plot local model data: Visualises the extracted results and optionally compares them to proxy reconstructions (see
281 example in Fig. 5). Available visualisations include line plots of the annual cycle at the user-specified location, grouped
282 by the various DeepMIP CO₂ levels (Fig. 5a), and a scatter plot of all simulated annual mean values against the respective
283 GMSTs or CO₂ concentrations of the model simulations. (Fig. 5b). The latter plot type can be useful to compare the
284 sensitivity of the model results at the local site against global climate signals. The simulated monthly and annual mean
285 model results can be visually compared against a local proxy reconstruction, either by manually specifying the mean and
286 standard deviation of the proxy data or by loading the respective values for locations from the DeepMIP proxy dataset
287 The user can zoom and pan within the interactive figures and download them in PNG and SVG format.

288 3. Map sites and boundary conditions: Plots paleogeographic maps of the chosen site. The user can choose between a
289 global map indicating the location of the study site or regional maps of the bathymetry, orography and land-sea mask on
290 the various native model grids (Fig. 6). The latter can help with the interpretation of the model-data comparison result,
291 e.g. by visualising local grid resolutions and associated intermodel differences in the representation of mountain ranges
292 or ocean gateways.

293 How to cite the dataset

294 This Data Descriptor paper should be cited whenever any netCDF files from the dataset or results from the web application are
295 reused in a publication. In addition, the user might want to cite the previously published overview of simulated large-scale
296 climate features¹³ or the DeepMIP-Eocene experimental design¹³ as appropriate.

297 Code availability

298 Processing code to interpolate model fields and to create the validation overview tables is available via Zenodo³⁷. The code for
299 the web application is deposited in a separate Zenodo repository³⁸.

300 References

301 1. Tierney, J. E et al. Past climates inform our future. *Science* 370, eaay3701, [10.1126/science.aay3701](https://doi.org/10.1126/science.aay3701) (2020).

- 302 2. Hollis, C. J. et al. The DeepMIP contribution to PMIP4: methodologies for selection, compilation and analysis of latest
303 Paleocene and early Eocene climate proxy data, incorporating version 0.1 of the DeepMIP database. *Model. Dev.*
304 12, 3149–3206, [10.5194/gmd-12-3149-2019](https://doi.org/10.5194/gmd-12-3149-2019) (2019). Publisher: Copernicus GmbH.
- 305 3. Burke, K. D. et al. Pliocene and Eocene provide best analogs for near-future climate. *Proc. Natl. Acad. Sci.* 115,
306 13288–13293, [10.1073/pnas.1809600115](https://doi.org/10.1073/pnas.1809600115) (2018).
- 307 4. Rae, J. W. et al. Atmospheric CO₂ over the Past 66 Million Years from Marine Archives. *Annu. Rev. Earth Planet. Sci.* 49,
308 609–641, [10.1146/annurev-earth-082420-063026](https://doi.org/10.1146/annurev-earth-082420-063026) (2021).
- 309 5. Inglis, G. N. et al. Global mean surface temperature and climate sensitivity of the early Eocene Climatic Optimum (EECO),
310 Paleocene–Eocene Thermal Maximum (PETM), and latest Paleocene. *Clim. Past* 16, 1953–1968, [10.5194/cp-16-1953-2020](https://doi.org/10.5194/cp-16-1953-2020)
311 (2020).
- 312 6. Heinemann, M., Jungclauss, J. H. & Marotzke, J. Warm Paleocene/Eocene climate as simulated in ECHAM5/MPI-OM.
313 *Clim. Past* 5, 785–802, [10.5194/cp-5-785-2009](https://doi.org/10.5194/cp-5-785-2009) (2009).
- 314 7. Roberts, C. D., LeGrande, A. N. & Tripathi, A. K. Climate sensitivity to Arctic seaway restriction during the early Paleogene.
315 *Earth Planet. Sci. Lett.* 286, 576–585, [10.1016/j.epsl.2009.07.026](https://doi.org/10.1016/j.epsl.2009.07.026) (2009).
- 316 8. Winguth, A., Shellito, C., Shields, C. & Winguth, C. Climate Response at the Paleocene–Eocene Thermal Maximum to
317 Greenhouse Gas Forcing—A Model Study with CCSM. *Clim. Past* 7, 2562–2584, [10.1175/2009JCLI3113.1](https://doi.org/10.1175/2009JCLI3113.1) (2010).
- 318 9. Lunt, D. J. et al. CO₂-driven ocean circulation changes as an amplifier of Paleocene-Eocene thermal maximum hydrate
319 destabilization. *Geology* 38, 875–878, [10.1130/G31184.1](https://doi.org/10.1130/G31184.1) (2010).
- 320 10. Huber, M. & Caballero, R. The early Eocene equable climate problem revisited. *Clim. Past* 7, 603–633, [10.5194/
321 cp-7-603-2011](https://doi.org/10.5194/cp-7-603-2011) (2011).
- 322 11. Lunt, D. J. et al. A model-data comparison for a multi-model ensemble of early Eocene atmosphere-ocean simulations:
323 EoMIP. *Clim. Past* 8, 1717–1736, [10.5194/cp-8-1717-2012](https://doi.org/10.5194/cp-8-1717-2012) (2012). ISBN: 1814-9340.
- 324 12. Lunt, D. J. et al. The DeepMIP contribution to PMIP4: experimental design for model simulations of the EECO, PETM,
325 and pre-PETM (version 1.0). *Geosci. Model. Dev.* 10, 889–901, [10.5194/gmd-10-889-2017](https://doi.org/10.5194/gmd-10-889-2017) (2017).
- 326 13. Lunt, D. J. et al. DeepMIP: model intercomparison of early Eocene climatic optimum (EECO) large-scale climate features
327 and comparison with proxy data. *Clim. Past* 17, 203–227, [10.5194/cp-17-203-2021](https://doi.org/10.5194/cp-17-203-2021) (2021).

- 328 14. Anagnostou, E et al. Proxy evidence for state-dependence of climate sensitivity in the Eocene greenhouse. *Nature Commun.*
329 11, 4436, [10.1038/s41467-020-17887-x](https://doi.org/10.1038/s41467-020-17887-x) (2020).
- 330 15. Kelemen, F. D. et al. Meridional Heat Transport in the DeepMIP Eocene Ensemble: Non-CO₂ Effects. *Paleoceanogr. Paleoclimatology*
331 38, e2022PA004607, [10.1029/2022PA004607](https://doi.org/10.1029/2022PA004607) (2023).
- 332 16. Goudsmit-Harzevoort, B et al. The Relationship Between the Global Mean Deep-Sea and Surface Temperature During the
333 Early Eocene. *Paleoceanogr. Paleoclimatology* 38, e2022PA004532, [10.1029/2022PA004532](https://doi.org/10.1029/2022PA004532) (2023).
- 334 17. Zhang, Y. et al. Early Eocene Ocean Meridional Overturning Circulation: The Roles of Atmospheric
335 Forcing and Strait Geometry. *Paleoceanogr. Paleoclimatology* 37, [10.1029/2021PA004329](https://doi.org/10.1029/2021PA004329) (2022). _eprint:
336 <https://onlinelibrary.wiley.com/doi/pdf/10.1029/2021PA004329>.
- 337 18. Niezgodzki, I. et al. Simulation of Arctic sea ice within the DeepMIP Eocene ensemble: Thresholds, seasonality and
338 factors controlling sea ice development. *Glob. Planet. Chang.* 214, 103848, [10.1016/j.gloplacha.2022.103848](https://doi.org/10.1016/j.gloplacha.2022.103848) (2022).
- 339 19. Williams, C. J. R. et al. African Hydroclimate During the Early Eocene From the DeepMIP Simulation. *Paleoceanogr.*
340 *Paleoclimatology* 37, [10.1029/2022PA004419](https://doi.org/10.1029/2022PA004419) (2022).
- 341 20. Reichgelt, T. et al. Plant Proxy Evidence for High Rainfall and Productivity in the Eocene of Australia. *Paleoceanogr.*
342 *Paleoclimatology* 37, [10.1029/2022PA004418](https://doi.org/10.1029/2022PA004418) (2022).
- 343 21. Cramwinckel, M. J. et al. Global and Zonal-Mean Hydrological Response to Early Eocene Warming. *Paleoceanogr.*
344 *Paleoclimatology* 38, e2022PA004542, [10.1029/2022PA004542](https://doi.org/10.1029/2022PA004542) (2023).
- 345 22. Kad, P., Blau, M. T., Ha, K.-J. & Zhu, J. Elevation-dependent temperature response in early Eocene using paleoclimate
346 model experiment. *Environ. Res. Lett.* 17, 114038, [10.1088/1748-9326/ac9c74](https://doi.org/10.1088/1748-9326/ac9c74) (2022). Publisher: IOP Publishing.
- 347 23. Zhang, Z. et al. Impact of Mountains in Southern China on the Eocene Climates of East Asia. *J. Geophys. Res. Atmospheres*
348 127, [10.1029/2022JD036510](https://doi.org/10.1029/2022JD036510) (2022). _eprint: <https://onlinelibrary.wiley.com/doi/pdf/10.1029/2022JD036510>.
- 349 24. Steinig, S. et al. Deep-Time Model Intercomparison Project (DeepMIP) Eocene model data version 1.0, [10.5285/
350 95AA41439D564756950F89921B6EF215](https://doi.org/10.5285/95AA41439D564756950F89921B6EF215) (2024).
- 351 25. Cinquini, L. et al. The Earth System Grid Federation: An open infrastructure for access to distributed geospatial data.
352 *Futur. Gener. Comput. Syst.* 36, 400–417, [10.1016/j.future.2013.07.002](https://doi.org/10.1016/j.future.2013.07.002) (2014).

- 353 26. Iturbide, M. et al. Implementation of FAIR principles in the IPCC: the WGI AR6 Atlas repository. *Sci. Data*9, 629,
354 [10.1038/s41597-022-01739-y](https://doi.org/10.1038/s41597-022-01739-y) (2022).
- 355 27. Herold, N. et al. A suite of early Eocene (55 Ma) climate model boundary conditions. *Geosci. Model. Dev.*7, 2077–2090,
356 [10.5194/gmd-7-2077-2014](https://doi.org/10.5194/gmd-7-2077-2014) (2014).
- 357 28. Baatsen, M. et al. Reconstructing geographical boundary conditions for palaeoclimate modelling during the Cenozoic.
358 *Clim. Past*12, 1635–1644, [10.5194/cp-12-1635-2016](https://doi.org/10.5194/cp-12-1635-2016) (2016). Publisher: Copernicus GmbH.
- 359 29. Kiehl, J. T. & Shields, C. A. Sensitivity of the Palaeocene–Eocene Thermal Maximum climate to cloud properties.
360 *Transactions Royal Soc. A: Math. Phys. Eng. Sci.* 20130093, [10.1098/rsta.2013.0093](https://doi.org/10.1098/rsta.2013.0093) (2013). Publisher: Royal Society.
- 361 30. Zhu, J., Poulsen, C. J. & Tierney, J. E. Simulation of Eocene extreme warmth and high climate sensitivity through cloud
362 feedbacks. *Sci. Adv.*1–11, [10.1126/sciadv.aax1874](https://doi.org/10.1126/sciadv.aax1874) (2019).
- 363 31. Hagemann, S. & Dümenil, L. A parametrization of the lateral water flow for the global ocean. *Climate Dyn.*14, 17–31,
364 [10.1007/s003820050205](https://doi.org/10.1007/s003820050205) (1998). ISBN: 0930-7575.
- 365 32. Zhang, Z. S. et al. Pre-industrial and mid-Pliocene simulations with NorESM. *Geosci. Model. Dev.*5, 523–533,
366 [10.5194/gmd-5-523-2012](https://doi.org/10.5194/gmd-5-523-2012) (2012).
- 367 33. Schulzweida, U. CDO User Guide, [10.5281/zenodo.7112925](https://doi.org/10.5281/zenodo.7112925) (2022). Publisher: Zenodo.
- 368 34. Hassell, D., Gregory, J., Blower, J., Lawrence, B. N. & Taylor, K. E. A data model of the Climate and Forecast
369 metadata conventions (CF-1.6) with a software implementation (cf-python v2.0). *Geosci. Model. Dev.*10, 4619–4646,
370 [10.5194/gmd-10-4619-2017](https://doi.org/10.5194/gmd-10-4619-2017) (2017).
- 371 35. Rew, R. et al. Unidata NetCDF, [10.5065/D6H70CW6](https://doi.org/10.5065/D6H70CW6) (1989). Language: en Medium: application/java-
372 archive,application/gzip,application/tar.
- 373 36. Steinig, S. sebsteinig/deepmip-web-app: as published in DeepMIP data descriptor paper (Scientific Data), [10.5281/
374 ZENODO.12706779](https://doi.org/10.5281/ZENODO.12706779) (2024).
- 375 37. Steinig, S. sebsteinig/deepmip-helpers: as published in DeepMIP data descriptor paper (Scientific Data), [10.5281/
376 ZENODO.12706785](https://doi.org/10.5281/ZENODO.12706785) (2024).
- 377 38. Zhang, Y. et al. Early Eocene vigorous ocean overturning and its contribution to a warm Southern Ocean. *Clim. Past*16,
378 1263–1283, [10.5194/cp-16-1263-2020](https://doi.org/10.5194/cp-16-1263-2020) (2020).

379 39. Zhang, Z. & Yan, Q. Pre-industrial and mid-Pliocene simulations with NorESM-L: AGCM simulation with the CESM1.0. *Geosci. Model.*
380 *Dev.* 5, 1033–1043, [10.5194/gmd-5-1033-2012](https://doi.org/10.5194/gmd-5-1033-2012) (2012).

381 Acknowledgements

382 Sebastian Steinig and Daniel J. Lunt acknowledge funding from the NERC SWEET grant (grant no. NE/P01903X/1). Daniel J.
383 Lunt also acknowledges funding from NERC DeepMIP grant (grant no. NE/N006828/1) and the ERC (“The greenhouse earth
384 system” grant; T-GRES, project reference no. 340923, awarded to Rich Pancost). The CESM project is primarily supported by
385 the National Science Foundation (NSF). This material is based upon work supported by the National Center for Atmospheric
386 Research, which is a major facility sponsored by the NSF under Cooperative Agreement No. 1852977. MIROC simulations
387 were supported by funding from KAKENHI grant no. 17H06104 and 17H06323. Gordon. N Inglis was supported by a Royal
388 Society Dorothy Hodgkin Fellowship (DHF/R1\191178) and NERC Large Grant (NE/V018388/1). Agatha de Boer and David
389 Hutchinson acknowledge support from Swedish Research Council Grant 2016-03912 and FORMAS grant 2018-0162. The
390 GFDL simulations were performed using resources from the Swedish National Infrastructure for Computing (SNIC) at the
391 National Supercomputer Centre (NSC), partially funded by the Swedish Research Council Grant 2018-05973.

392 Author contributions statement

393 The model simulations and individual post-processing were carried out by JZ and CJP (CESM), IN and GK (COSMOS), DKH
394 and AMdB (GFDL), SS and DJL (HadCM3), PM and EMV (INMCM), JBL and YD (IPSL), WLC and AAO (MIROC), and
395 ZZ (NorESM). DE, GNI and ANM provided input on the web application and proxy data implementation. SS compiled the
396 global dataset and developed the web application. SS wrote the manuscript with contributions from all authors.

397 Competing interests

398 The authors declare no competing interests relevant to this study.

Table 1. Summary of the available DeepMIP-Eocene model simulations in version 1.0 of the dataset. Experiment short names are defined in Table 2 and paleogeographies are shown in Fig. 1.

Model	Family	PI	1	1.5	2	3	4	6	9	Geography	Reference
CESM1.2-CAM5	CESM									27	13,30
COSMOS-landveg-r2413	COSMOS									27	13
GFDL-CM2.1	GFDL									27	13
HadCM3B-M2.1aN	HadCM3									27	13
HadCM3BL-M2.1aN	HadCM3									27	13
INM-CM4-8	INMCM									27	13
IPSLCM5A2	IPSL									27	13,38
MIROC4m	MIROC									27	13
NorESM1-F	NorESM									28	13

Table 2. Overview of the DeepMIP-Eocene experiments included in version 1.0 of the dataset.

Experiment Name	Short Name	CO ₂ [ppmv]	Geography
deepmip-eocene-p1-PI	PI	280	modern
deepmip-eocene-p1-x1	x1	280	27 or 28
deepmip-eocene-p1-x1.5	x1.5	420	27 or 28
deepmip-eocene-p1-x2	x2	560	27 or 28
deepmip-eocene-p1-x3	x3	840	27 or 28
deepmip-eocene-p1-x4	x4	1120	27 or 28
deepmip-eocene-p1-x6	x6	1680	27 or 28
deepmip-eocene-p1-x9	x9	2520	27 or 28

Table 3. Overview of initial ocean temperature strategies. Coefficients A, B and D refer to Eq. (1).

Model	A	B	D	Comment
CESM1.2-CAM5	–	–	–	from previous CCSM3 simulation ²⁹
COSMOS-landveg-r2413	–	–	–	10 °C globally
GFDL-CM2.1	25	10	5000	
HadCM3B-M2.1aN	–	–	–	branched from HadCM3BL
HadCM3BL-M2.1aN	–	–	–	custom equations ¹³
INM-CM4-8	20	15	5000	
IPSLCM5A2	25	10	1000	
MIROC4m	25	0	5000	
NorESM1-F	–	–	–	from previous NorESM-L simulation ³⁹
experimental design ²⁷	25	15	5000	

Table 4. Atmosphere output variables included in version 1.0 of the dataset. Naming conventions follow the CMIP6 data request.

Name	Long Name	Units	Dimensions
tas	Near-Surface Air Temperature	K	time lat lon
ts	Surface Temperature	K	time lat lon
pr	Precipitation	kg m ² s ⁻¹	time lat lon
evspsbl	Evaporation Including Sublimation and Transpiration	kg m ² s ⁻¹	time lat lon
h s	Surface Upward Latent Heat Flux	W m ²	time lat lon
hfss	Surface Upward Sensible Heat Flux	W m ²	time lat lon
ps	Surface Air Pressure	Pa	time lat lon
psl	Sea Level Pressure	Pa	time lat lon
snc	Snow Area Fraction	%	time lat lon
rsds	Surface Downwelling Shortwave Radiation	W m ²	time lat lon
rlds	Surface Downwelling Longwave Radiation	W m ²	time lat lon
rsus	Surface Upwelling Shortwave Radiation	W m ²	time lat lon
rlus	Surface Upwelling Longwave Radiation	W m ²	time lat lon
rsdt	TOA Incident Shortwave Radiation	W m ²	time lat lon
rsut	TOA Outgoing Shortwave Radiation	W m ²	time lat lon
rlut	TOA Outgoing Longwave Radiation	W m ²	time lat lon
rsdscs	Surface Downwelling Clear-Sky Shortwave Radiation	W m ²	time lat lon
rldscs	Surface Downwelling Clear-Sky Longwave Radiation	W m ²	time lat lon
rsuscscs	Surface Upwelling Clear-Sky Shortwave Radiation	W m ²	time lat lon
rluscscs	Surface Upwelling Clear-Sky Longwave Radiation	W m ²	time lat lon
rsutscs	TOA Outgoing Clear-Sky Shortwave Radiation	W m ²	time lat lon
rlutscs	TOA Outgoing Clear-Sky Longwave Radiation	W m ²	time lat lon
tauu	Surface Downward Eastward Wind Stress	Pa	time lat lon
tauv	Surface Downward Northward Wind Stress	Pa	time lat lon
uas	Eastward Near-Surface Wind	W m ²	time lat lon
vas	Northward Near-Surface Wind	W m ²	time lat lon
clh	High Level Cloud Fraction	%	time lat lon
clm	Mid Level Cloud Fraction	%	time lat lon
cll	Low Level Cloud Fraction	%	time lat lon
clt	Total Cloud Cover Percentage	%	time lat lon
cl	Percentage Cloud Cover	%	level time lat lon
hus	Specific Humidity	1	level time lat lon
ta	Air Temperature	K	level time lat lon
ua	Eastward Wind	m s ⁻¹	level time lat lon
va	Northward Wind	m s ⁻¹	level time lat lon
wap	Omega (=dp/dt)	Pa s ⁻¹	level time lat lon
zg	Geopotential Height	m	level time lat lon
orog	Surface Altitude	m	lat lon
sftlf	Percentage of the Grid Cell Occupied by Land	%	lat lon

Table 5. Ocean output variables included in version 1.0 of the dataset. Naming conventions follow the CMIP6 data request.

Name	Long Name	Units	Dimensions
tos	Sea Surface Temperature	C	time lat lon
siconc	Sea-Ice Area Percentage (Ocean Grid)	%	time lat lon
m1otst	Ocean Mixed Layer Thickness Defined by Sigma T	m	time lat lon
zos	Sea Surface Height Above Geoid	m	time lat lon
hfds	Downward Heat Flux at Sea Water Surface	W m ²	time lat lon
wfo	Water Flux Into Sea Water	kg m ² s ⁻¹	time lat lon
tauuo	Sea Water Surface Downward X Stress	N m ⁻²	time lat lon
tauvo	Sea Water Surface Downward Y Stress	N m ⁻²	time lat lon
msftbarot	Ocean Barotropic Mass Streamfunction	kg s ⁻¹	time lat lon
msftmz	Ocean Meridional Overturning Mass Streamfunction	kg s ⁻¹	time depth lat
so	Sea Water Salinity	0:001	depth time lat lon
thetao	Sea Water Potential Temperature	C	depth time lat lon
uo	Sea Water X Velocity	m s ⁻¹	depth time lat lon
vo	Sea Water Y Velocity	m s ⁻¹	depth time lat lon
wo	Sea Water Vertical Velocity	m s ⁻¹	depth time lat lon
difvmo	Ocean Vertical Momentum Diffusivity	m ² s ⁻¹	depth time lat lon
difvtrbo	Ocean Vertical Tracer Diffusivity Due to Background	m ² s ⁻¹	depth time lat lon
deptho	Sea Floor Depth Below Geoid	m	lat lon

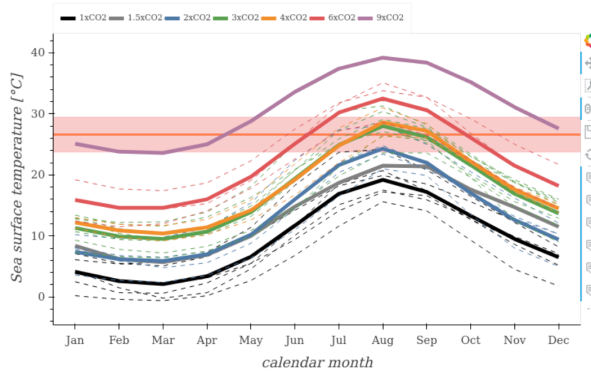
Figure 1. Comparison of available DeepMIP-Eocene paleogeographic boundary conditions. Orography and bathymetry are based on published reconstruction²⁷ (a) and are also available based on a palaeomagnetic reference frame²⁸ (b) with differences in the relative positions of plates (c).

Figure 2. Technical validation of atmospheric global model fields of the experiment across the ensemble. Variables with multiple vertical levels are shown for the respective model pressure level closest to 500 hPa. Tables for other experiments and "time_series" files can be found in the web application at https://data.deepmip.org/Validation_tables. Note that the INM and NorESM models did not perform the experiment (Table 1) and are therefore excluded from this analysis.

Figure 3. Technical validation of ocean global model fields of the experiment across the ensemble. Variables with multiple vertical levels are shown for the respective model depth closest to 1000 m. Tables for other experiments and "time_series" files can be found in the web application at https://data.deepmip.org/Validation_tables. Note that the INM and NorESM models did not perform the experiment (Table 1) and are therefore excluded from this analysis.

Figure 4. Example user input and extracted model data for a single site in the web application.

(a) DeepMIP Sea surface temperature (annual cycle)
 site: Store Bælt (Denmark) (plat = 48.4 / plon = 7.4)
 solid lines: ensemble mean / dashed lines: individual models



(b) DeepMIP Sea surface temperature (annual mean)
 site: Store Bælt (Denmark) (plat = 48.4 / plon = 7.4)

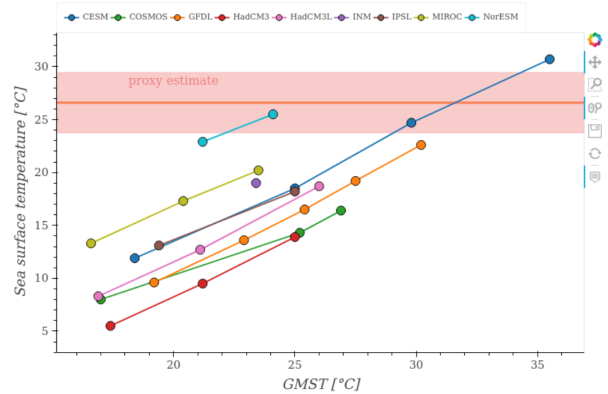


Figure 5. Example graphical output of the web application for the model-data comparison of the Store Bælt (Denmark) site defined in Fig. 4. (a) Simulated annual cycle of sea surface temperatures at the respective grid point closest to the reconstructed paleoposition of the site. Solid lines show the ensemble mean for each CO₂ concentration with individual models represented by the dashed lines. (b) Scatter plot of the simulated annual mean sea surface temperature at the proxy site compared to the global mean surface temperature of the respective simulation. Lines connect results of the same model. Reconstructed proxy temperature is based on the TEX₈₆ paleothermometer².

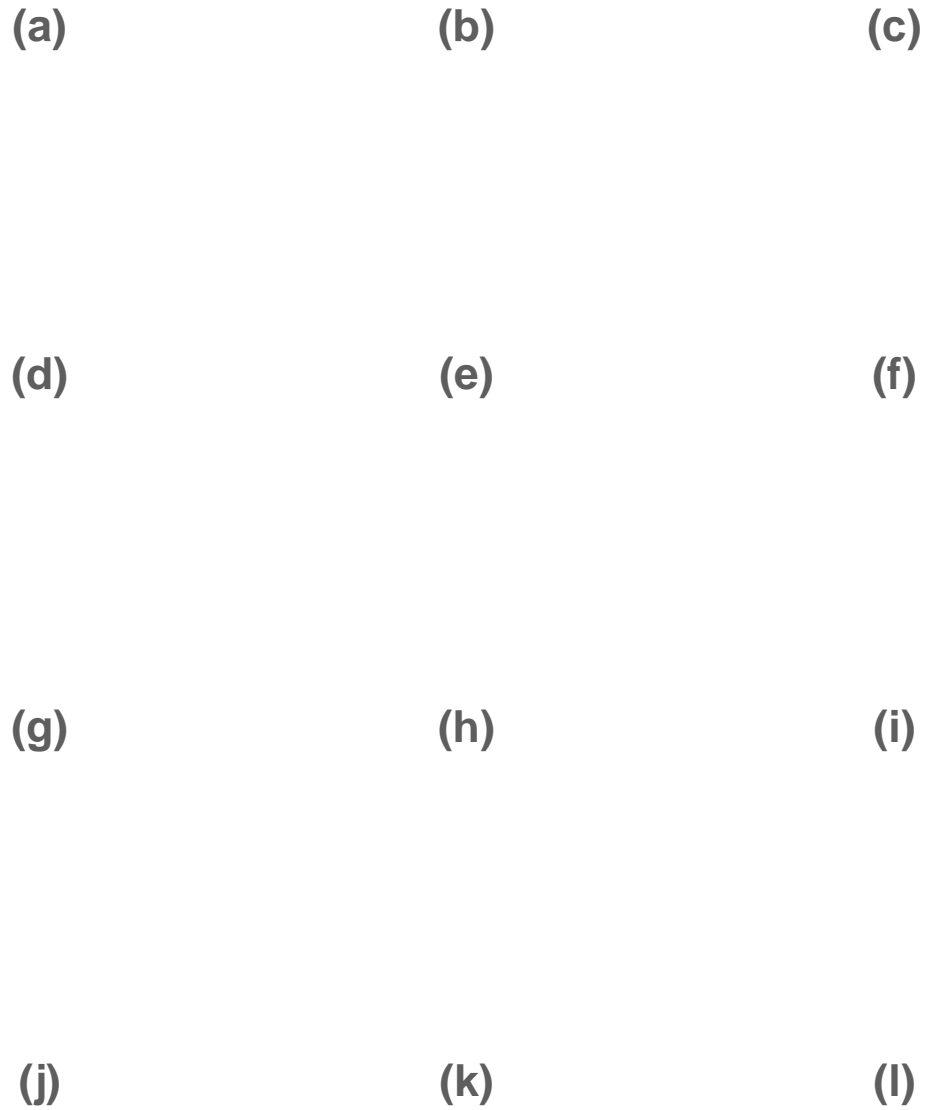


Figure 6. Maps of local boundary condition differences between some of the models around the the Store Bælt (Denmark) site defined in Fig. 4 produced by the web application. The reconstructed paleoposition of the site (red dot) represents a land point in COSMOS (panel d-f) and ocean points in the other models. Note the different paleogeographic reconstruction used in NorESM (panel j-l).